Journal of Low Temperature Physics, Vol. 138, Nos. 5/6, March 2005 (© 2005)
DOI: 10.1007/s10909-004-2893-0

^{3}He Impurities in ^{4}He Systems Adsorbed on Curved Substrates

S. A. Sartarelli,[1] L. Szybisz,[2,3] and E. S. Hernández[2]

[1]*Instituto de Ciencias, Universidad Nacional de General Sarmiento, RA-1663 San Miguel, Argentina*
[2]*Departamento de Física, Facultad de Ciencias Exactas y Naturales, Universidad de Buenos Aires, RA-1428 Buenos Aires, Argentina, and Consejo Nacional de Investigaciones Científicas y Técnicas, Argentina*
E-mail: shernand@df.uba.ar
[3]*Laboratorio Tandar, Comisión Nacional de Energía Atómica, Av. del Libertador 8250, RA-1429 Buenos Aires, Argentina*

(Received August 28, 2004; revised October 19, 2004)

It is shown that ^{3}He impurities in sufficiently large ^{4}He systems adsorbed onto substrates with curved geometries form surface bound states, analogous to the Andreev state on a planar liquid–vapor interface. We report the analysis performed for superfluid ^{4}He adsorbed on the external surface of the nano-fullerene C_{60} and on cylindrical nano-wires of Au. It is found that a single ^{3}He impurity diluted into such adsorbed structures behaves as on films on planar substrates and as on pure ^{4}He clusters.

KEY WORDS: substrates; ^{3}He impurities; Andreev state.

1. INTRODUCTION

During the last two decades, a large amount of work has been devoted to investigate the adsorption of quantum fluids in restricted geometries.[1] In particular, experimental and theoretical studies of the behavior of a single ^{3}He impurity adsorbed into the ^{4}He fluid have been issues of great interest. Since ^{3}He and ^{4}He atoms interact through the same potential, the properties of their mixed systems are determined by quantum effects.[2] In this case, the zero point motion becomes very important. Let us mention that impurities heavier than helium atoms (e.g., alkali metals or the SF_6 molecule), for which one expects a small zero point motion, can be treated as classical objects in a quantum fluid.[3–5] One ^{3}He

atom, being lighter than ^{4}He, tends to move in regions of low ^{4}He density. This feature leads to the so-called Andreev state of ^{3}He on a ^{4}He liquid–vapor interface at low temperature.[6] Several theoretical descriptions of finite helium systems such as films and clusters have shown the same kind of localization. Microscopic calculations of ^{3}He impurities on helium films adsorbed on a planar graphite surface, performed within the variational hypernetted-chain equations (HNC) theory by Krotscheck and coworkers,[7–9] showed the structure and energetics of states localized at the outer film surface for various ^{4}He coverages. Pavloff and Treiner[10] found similar structures applying finite range density functional theory (FRDF) to ^{3}He atoms in films of liquid ^{4}He adsorbed on planar Nuclepore. Density functional (DF) theory applied to ^{4}He clusters also demonstrated this localization; Dalfovo[11] employed a zero-range DF to describe both the ^{4}He drops and the ^{3}He–^{4}He interaction and later, within a similar FRDF approach, Barranco *et al.*[14] computed the energetics of these impurities in pure and doped ^{4}He clusters. Moreover, variational Monte Carlo (VMC) calculations for ^{3}He adatoms on ^{4}He$_N$ droplets have been carried out by Belić *et al.* [13] In all calculations, one finds indications that as the finite ^{4}He system grows towards the thermodynamic limit, the energy of the impurity also approaches a limiting value. Within some dispersion attributable to the different methods employed, these asymptotic values seem to appear in the vicinity of -5 K, the experimental value originally reported by Edwards and Saam.[2]

Quite recently, FRDF's have been applied to study adsorption of ^{4}He on curved substrates, in particular, on strongly attractive spherical carbon fullerenes[15,16] and on cylindrical metallic nano-wires.[17] In such a theory the ground-state (gs) energy of an interacting N-body system of ^{4}He atoms, confined by an adsorbate-substrate potential $U_{\rm sub}(\mathbf{r})$, may be written as

$$E_{\rm gs} = -\frac{\hbar^2}{2m}\int d\mathbf{r}\sqrt{\rho_4(\mathbf{r})}\nabla^2\sqrt{\rho_4(\mathbf{r})} + \int d\mathbf{r}\rho_4(\mathrm{r})\mathrm{e}_{\rm cor}(\mathbf{r}) + \int \mathbf{dr}\rho_4(\mathbf{r})\mathbf{U}_{\rm sub}(\mathbf{r}), \tag{1.1}$$

where $\rho_4(\mathbf{r})$ is the one-body density and $\mathrm{e}_{\rm cor}(\mathbf{r})$ the correlation energy per particle. The density profile $\rho_4(\mathbf{r})$ is determined from the Euler–Lagrange (EL) equation derived from the condition

$$\frac{\delta\Omega}{\delta\rho_4(\mathbf{r})} = \frac{\delta\left\{E_{\rm gs}[\rho_4, \nabla\rho_4] - \mu N\right\}}{\delta\rho_4(\mathbf{r})} = 0 \tag{1.2}$$

in the respective geometry.

In the spirit of these previous works we now focus on the effects of the finite substrate curvature on the ^{3}He impurities in the adsorbed ^{4}He shells. Accordingly, in the present work we report a study of the adsorption of a single ^{3}He atom on $^4\mathrm{He}_N + \mathrm{C}_{60}$ clusters by employing for ^{4}He the FRDF proposed by the Orsay–Trento (OT) collaboration,[18] and on ^{4}He shells that coat cylindrical Au nano-wires as described in Ref. 17. For this sake, in Sec. 2 we shortly review the DF formalism and some particular geometrical details, and in Sec. 3 we discuss our main results. We also show that the overall picture is the same in spherical and cylindrical geometries, and discuss the energy systematics for ^{3}He in both cases. The summary and outlook are presented in Sec 4.

2. DENSITY FUNCTIONAL FORMALISM FOR ^{4}HE FILMS WITH ONE ^{3}HE IMPURITY IN CURVED GEOMETRIES

Within DF theory, the density profiles $\rho_4(\mathbf{r})$ of ^{4}He in any specific geometry are obtained solving a Hartree equation

$$-\frac{\hbar^2}{2m_4}\nabla^2\sqrt{\rho_4(\mathbf{r})} \tag{2.1}$$

$$+[V_H(\mathbf{r}) + U_{\mathrm{sub}}(\mathbf{r})]\sqrt{\rho_4(\mathbf{r})} = \mu_4\sqrt{\rho_4(\mathbf{r})}, \tag{2.2}$$

which also determines the chemical potential of helium atoms μ_4. Here $V_H(\mathbf{r})$ is a Hartree mean-field potential given by the first functional derivative of the total correlation energy $E_{sc}[\rho]$.

$$V_H(\mathbf{r}) = \frac{\delta E_{sc}[\rho]}{\delta\rho_4(\mathbf{r})} = \frac{\delta}{\delta\rho_4(\mathbf{r})}\int d\mathbf{r}'\rho_4(\mathbf{r}')\mathbf{e_{cor}}(\mathbf{r}'). \tag{2.3}$$

When one considers a ^{3}He impurity in the ^{4}He fluid, the single particle (sp) wave functions ϕ_α are optimally calculated by solving the equation

$$\left[-\nabla\frac{\hbar^2}{2m_3^*}\nabla + V_3(\mathbf{r}) + U_{\mathrm{sub}}(\mathbf{r})\right]\phi_\alpha = \varepsilon_\alpha\phi_\alpha, \tag{2.4}$$

where m_3^* is the effective mass of the ^{3}He atoms in ^{4}He

$$\frac{\hbar^2}{2m_3^*} = \frac{\hbar^2}{2m_3}\left(1 - \frac{\bar{\rho}_4(\mathbf{r})}{\rho_{4c}}\right)^2 \tag{2.5}$$

with $\rho_{4c} = 0.062\,\text{Å}^{-3}$. Here $\bar{\rho}_4(\mathbf{r})$ is the usual coarse-grained density[18] obtained by averaging the actual density $\rho_4(\mathbf{r})$ within a sphere of radius h with constant weighting function $w_4(|\mathbf{r}-\mathbf{r}'|)$. The quantity $V_3(\mathbf{r})$ is an

effective potential univocally determined by the ^{4}He gs density through the DF as

$$\begin{aligned} V_3(\mathbf{r}) &= \int d\mathbf{r}'\rho_4(\mathbf{r}')\{V_{34}(|\mathbf{r}-\mathbf{r}'|) \\ &\quad + w_3(|\mathbf{r}-\mathbf{r}'|)\bar{\rho}_4(\mathbf{r}')[c_4' + c_4''\bar{\rho}_4(\mathbf{r}')] \\ &\quad + c_{34}\rho_4(\mathbf{r})\bar{\rho}_4(\mathbf{r})^{\gamma_{34}}\}, \end{aligned} \tag{2.6}$$

where w_3 is the coarse graining weighting function for the ^{3}He atom density and the remaining quantities are the same as in Ref. 14. In other words, the mean field $V_3(\mathbf{r})$ is that given by the DF description of mixtures of helium isotopes[14,19,20] after setting the particle and kinetic energy densities of the ^{3}He fluid equal to zero.[21]

2.1. Spherical Geometry

In Refs. 15 and 16, Eq. (2.2) was solved for a wide range of fixed numbers of helium atoms N in $^4\mathrm{He}_N + \mathrm{C}_{60}$ clusters, such that

$$N = 4\pi \int_0^\infty r^2\, dr\, \rho_4(r). \tag{2.7}$$

This enables us to compute the mean field (2.6) and investigate the binding of a single ^{3}He atom to those systems. In the spherical geometry one can expand ϕ_α in spherical harmonics. The generic impurity state will be characterized by a principal quantum number n and the angular momentum l

$$\phi_\alpha = \frac{\mathcal{R}_{nl}(r)}{r} Y_{lm}(\hat{r}). \tag{2.8}$$

Schrödinger equation for the generic radial wave function $\mathcal{R}_{nl}$ is

$$\begin{aligned} &-\frac{\hbar^2}{2m_3^*}\frac{d^2}{dr^2}\mathcal{R}_{nl} - \left(\frac{d}{dr}\frac{\hbar^2}{2m_3^*}\right)\frac{d}{dr}\mathcal{R}_{nl} \\ &+\left[V_3(r) + \frac{1}{r}\left(\frac{d}{dr}\frac{\hbar^2}{2m_3^*}\right) + \frac{\hbar^2}{2m_3^*}\frac{l(l+1)}{r^2} + U_{\mathrm{sub}}(r)\right]\mathcal{R}_{nl} = \varepsilon_{nl}\mathcal{R}_{nl}. \end{aligned} \tag{2.9}$$

and the probability density $|\mathcal{R}_{nl}(r)|^2$ is normalized according to

$$\int_0^\infty dr|\mathcal{R}_{nl}(r)|^2 = 1. \tag{2.10}$$

2.2. Cylindrical Geometry

In Ref. 17, density profiles and energy systematics of fluid ^{4}He adsorbed on Au nano-wires have been presented. In this case, the ^{4}He density is normalized so as to define an areal coverage n_4 on a tube of radius R and length L

$$n_4 = \frac{N}{2\pi RL} = \frac{1}{R}\int_0^\infty r\,dr\,\rho_4(r) \tag{2.11}$$

and the single atom wave function for ^{3}He is

$$\phi_\alpha = \frac{\mathcal{R}_{nlk}(r)}{\sqrt{r}}\frac{e^{i(kz+l\varphi)}}{2\pi L}, \tag{2.12}$$

where

$$\int_0^\infty dr|\mathcal{R}_{nlk}(r)|^2 = 1. \tag{2.13}$$

For band heads nl with axial momentum $k=0$, the Schrödinger equation is the same as Eq. (2.9), with a centrifugal potential of intensity $l^2-1/4$.

3. NUMERICAL RESULTS AND ANALYSIS

As a first step, we have solved the Schrödinger equation (2.9) for a single ^{3}He atom in the mean field $V_3(r)+U_{\rm sub}(r)$, with $U_{\rm sub}(r)$ being the outer spherical potential created by a C_{60} fullerene.[15,16] The densities $\rho_4(r)$ for the different numbers N of ^{4}He atoms are those in Ref. 16, computed with the complete OT density functional. Due to the fact that the centrifugal potential in Eq. (2.9) is scarcely effective at the distances where the sp wave functions localize, the states of the impurity group into rotational bands with spectrum

$$\varepsilon_{nl} = \varepsilon_{n0} + \frac{\hbar^2}{2m^*_{n0}r^2_{n0}}l^2 \tag{3.1}$$

and wave functions $\mathcal{R}_{nl}\equiv\mathcal{R}_{n0}$. As in previous works where this effect was reported[15,22,23] the spectral parameters m^*_{n0} and r_{n0} obtained by a fit to the computed spectrum are well reproduced by an averaged effective mass

$$\frac{1}{m^*_{n0}} = \int dr\,|\mathcal{R}_{n0}(r)|^2\,\frac{1}{m^*(r)} \tag{3.2}$$

and by the mean radius of the ^{4}He system, respectively.

Figure 1 shows the energy per particle $E_{\rm gs}/N$ and the chemical potential μ_4 in $^4{\rm He}_N + C_{60}$ clusters together with the sp energies of states 1s, 2s,

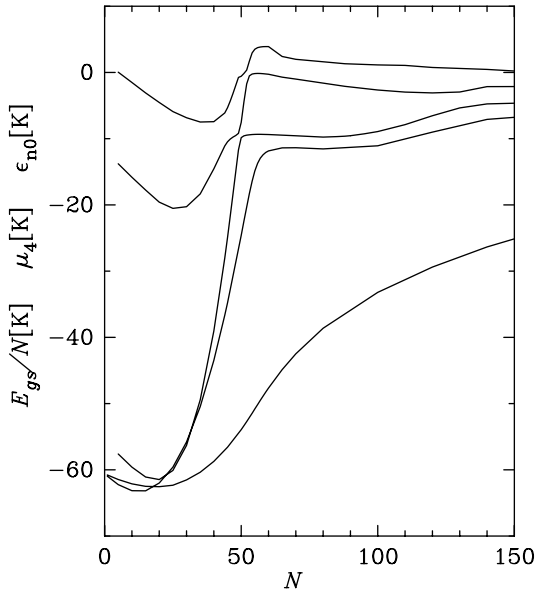

Fig. 1. From bottom to top (for $N > 40$) the curves, respectively, represent, in K, the energy per particle E_{gs}/N, the chemical potential μ_4, and the sp energies of states 1s, 2s, and 3s of one ^{3}He atom, as functions of N in doped ^4He_N+C_{60} clusters. These results were obtained with the complete Orsay–Trento functional.

and 3s of the ^{3}He impurity, all these as functions of N. In this figure we can observe a strong level repulsion near $N = 50$, immediately below promotion to a second layer in the ^{4}He shell. To analyze this effect, in Fig. 2 we plot the radial wave functions $\mathcal{R}_{10}(r)$ and $\mathcal{R}_{20}(r)$ versus the radial distance r for $N = 49$ (lower panel) and 50 (upper panel). In each plot, we also show the density $\rho_4(r)$ of the ^{4}He shell and the total one body field $V_3(r) + U_{sub}(r)$ experienced by the ^{3}He impurity. The horizontal full and dashed lines respectively indicate the energies ε_{10} and ε_{20} of the corresponding sp state. We clearly appreciate the very strong effect of the level repulsion identified in Fig. 1, that exchanges the localization of the gs and first excited sp wave functions, while the ^{4}He density stays in the submonolayer regime; for all particle numbers N above 50, the gs of the impurity remains localized at the outer surface of the ^{4}He spherical film. This is illustrated in Fig. 3, where the same curves are displayed for a thick shell with $N = 1000$, which displays a broad bulk-like region at practically constant saturation density $\rho_0 = 0.022\,\text{Å}^{-3}$. In this case, the wide potential well at the outer surface localizes both the gs and the excited wave function of the ^{3}He atom. Note, however, that although

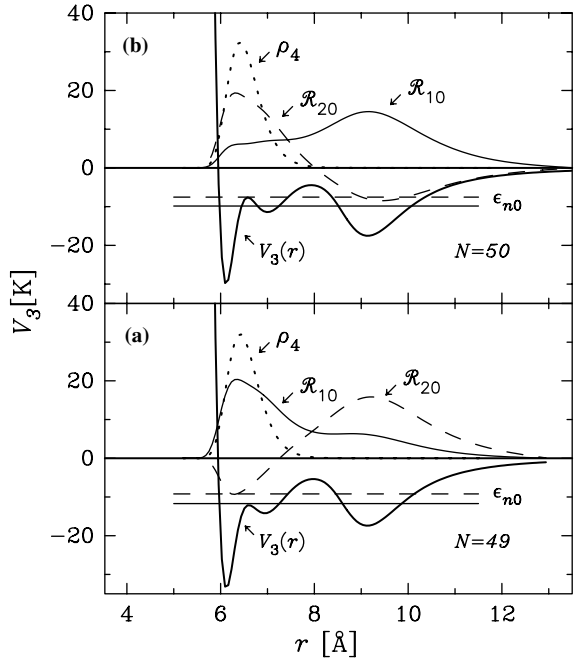

Fig. 2. Radial wave functions $\mathcal{R}_{n0}$ of one ^{3}He impurity and particle density of the adsorbed ^{4}He fluid, together with the respective mean fields (in K) experienced by the atoms for $N=49$ and 50. The functions $\rho_4(r)$ and $\mathcal{R}_{n0}(r)$ are displayed in arbitrary scales to fit in the plot. The horizontal lines respectively indicate the energy of the state. Note that the origin of the horizontal axis has been shifted to the radius of the C_{60} fullerene, 3.55 Å.

the gs state does not penetrate the film, the first excited state exhibits a finite probability density in the interior of the cluster. In fact, as the ^{4}He system approaches the thermodynamic limit, the whole set of excited states should evolve asymptotically into the state of the impurity dissolved in bulk ^{4}He,[10,14], with energy around -2.79 K according to experimental determinations.[24]

In Fig. 4 we plot (in triangles, see caption for details) the energies of the spherical Andreev states obtained in this work, together with previous DF results for spherical helium clusters, as functions of $N^{1/3}$. Note that for a fluid shell on a sphere of radius R, one can define a hydrodynamic radius a by the relation $N=4\pi\rho_0(a^3-R^3)/3$, with ρ_0 the bulk density of the liquid.[25] This means that for the largest N values where $a \gg R$, the variable in abscissae is essentially the curvature at the surface of the cluster, while for small particle numbers, $N^{-1/3}$ is very sensitive to the substrate curvature $1/R$. From this figure, we realize that a comparison

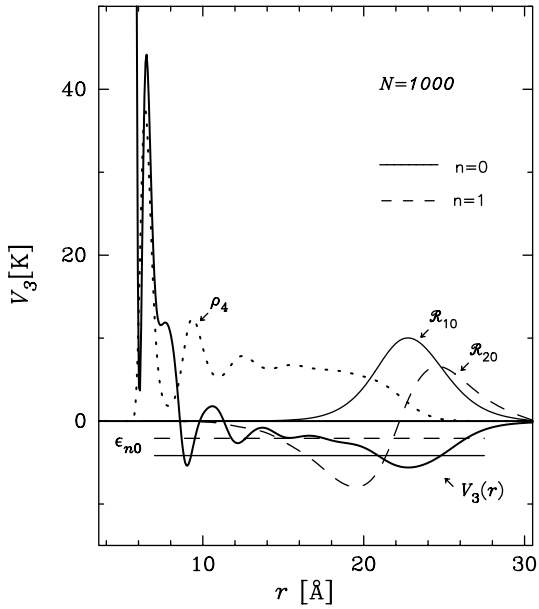

Fig. 3. Same as Fig. 2 for $N = 1000$.

between Andreev-like states in pure ^{4}He drops and in ^{4}He shells is meaningless for $N^{-1/3}$ above 0.14, i.e., for particle numbers below 360 atoms. In other words, for these small to moderate particle numbers, the ^{4}He shell does not screen the substrate, which strongly influences the impurity state. Instead, the results for the largest systems practically lie on a straight line, as is the case for the ^4He_N clusters where no extended substrate is present. The displayed dashed line corresponds to a least square fit to the data for $N > 500$ and crosses the vertical axis at -4.9 K, very close to the early reference value -5 K for the Andreev state in semiinfinite helium, indicated by the star. The coincidence between the trends of the open and the closed triangles indicates that the nonlocal kinetic energy effects of the OT functional[18] are not significant for the structure and energetics of the single ^{3}He impurity.

A characteristic of the present and previous DF calculations, visible in Fig. 4, is the fact that for any finite curvature the gs energy of the impurity lies above that of the Andreev state at the free surface of semi-infinite ^{4}He. This is mostly a manifestation of the substrate curvature, rather than an effect of the film structure, as supported by the following argument. The adsorbing potential exerted by a spherical surface of radius R, whose uniformly distributed atoms (at areal density θ) inter-

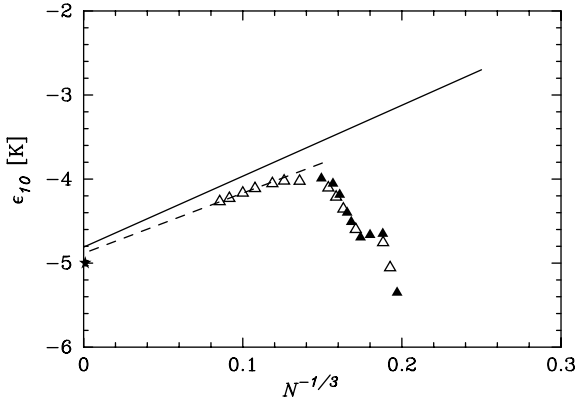

Fig. 4. Binding energy of the lowest impurity state as a function of $N^{-1/3}$. The star is the reference energy of the Andreev state according to Ref. 2. The solid line corresponds to the results of Ref. 14, the open triangles and dashed line (see text) to the results calculated by using OT-NLDF with $\alpha_s = 0$ and the full triangles to data evaluated with the complete OT-NLDF.

act pairwise with the adsorbate via a Lennard–Jones (*LJ*) potential of well depth ε_{LJ} and hard core $\sigma_{L,J}$, can be written as[15]

$$U_{\text{sub}}(r) = 4\pi\theta R^2 \varepsilon_{LJ} \frac{1}{Rr} \left\{ \frac{\sigma_{LJ}^{12}}{5} \left[\frac{1}{(r-R)^{10}} - \frac{1}{(r+R)^{10}} \right] - \frac{\sigma_{LJ}^{6}}{2} \left[\frac{1}{(r-R)^4} - \frac{1}{(r+R)^4} \right] \right\}. \tag{3.3}$$

For very large radius R, we find the planar limit

$$U_{\text{sub}}(z) = 4\pi\theta\varepsilon_{LJ} \left(\frac{\sigma_{LJ}^{12}}{5z^{10}} - \frac{\sigma_{LJ}^{6}}{2z^4} \right) \tag{3.4}$$

with positive $z = r - R \ll R$. As a consequence, we may write, in the small curvature regime

$$\begin{aligned} U_{\text{sub}}(r) &= U_{\text{sub}}(z) \left(1 - \frac{z}{R} + \frac{z^2}{R^2} + \cdots \right) + O\left(R^{-4}\right) \\ &= U_{\text{sub}}(z) + \delta U(z, R). \end{aligned} \tag{3.5}$$

To lowest order in the perturbation δU, discarding modifications in the density profile of the ^{4}He atoms introduced by a small finite curvature

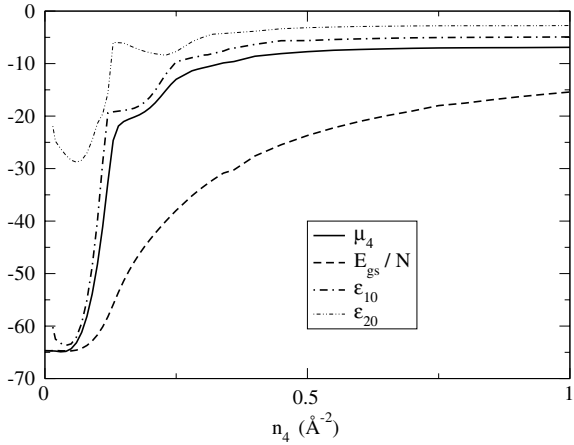

Fig. 5. Chemical potential and energy per particle of fluid ^{4}He adsorbed on an Au nano-wire of radius 12 Å, computed as in Ref. 17, gs energy and energy of the first excited state of a single ^{3}He atom, as functions of the areal coverage of ^{4}He atoms. All energies are given in K.

$1/R$, the change in the energy $\delta\varepsilon_0 = \varepsilon_0(R) - \varepsilon_0$ of the gs Andreev-like state is then

$$\delta\varepsilon_0 = \langle\Psi_0| - \frac{z}{R} U_{\text{sub}}(z)|\Psi_0\rangle \tag{3.6}$$

with $\Psi_0(z)$ the gs wave function in the planar limit. For a thin planar film, the Andreev state localizes in its bulk near the minimum of the potential well, that is essentially provided by the substrate. For a thick planar film with a well developed bulk region and free surface, $\Psi_0(z)$ is localized at a position z_f at the surface and is bound by the potential well created by the interaction with the ^{4}He atoms. In this situation, the full mean field $U_{\text{sub}} + V_3$ should enter (3.6); in either case, the correction $\delta\varepsilon_0$ is a positive linear function of curvature, as viewed in Fig. 4.

As a second step, we have tested the general features of this systematics in the cylindrical geometry. In Fig. 5 we display the chemical potential and energy per particle of fluid ^{4}He adsorbed on an Au nano-wire of 12 Å radius as computed in Ref. 17, together with the gs and first excited sp energies of a single ^{3}He atom, as functions of the areal coverage n_4. We mention here that the depth of the effective physisorption potential of gold is about one half that of graphite,[17] and that the abilities of FRDF's to describe wetting properties of helium on weak and moderate adsorbers have been favorably checked against Path Integral Monte Carlo calculations in a recent article.[26] The current energy pattern is very similar to

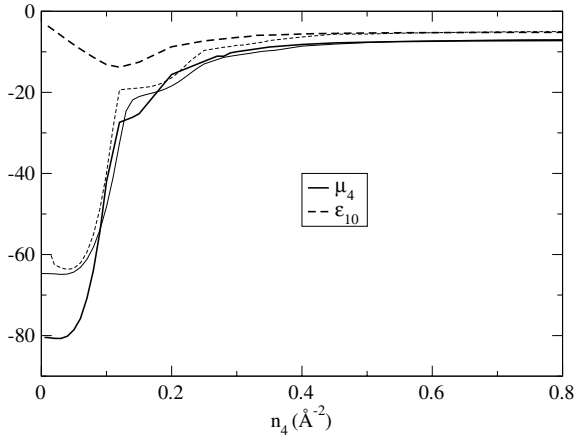

Fig. 6. Chemical potential of the ^{4}He fluid and gs energy of the ^{3}He impurity on semi-infinite solid Au (thick lines) and on a 12 Å radius Au tube (thin lines).

that in Fig. 1, including the level repulsion effect, that we have corroborated by inspection of the density profiles such as those in Fig. 2. Moreover, as in the spherical case, there is a clear asymptotic behavior of the 1s energies towards a value near $\varepsilon_0 \approx -5$ K, the energy of the Andreev state. The present calculations yield $\varepsilon_0 \simeq -4.88$ K when data of $^4\mathrm{He}_N + \mathrm{C}_{60}$ clusters with $N > 800$ (i.e., $N^{-1/3} < 0.108$) are extrapolated and $\varepsilon_0 \simeq -5.2$ K for the helium shell on an Au nano-wire with coverage $n_4 = 1.5\,\text{Å}^{-2}$. Correspondingly, our curves for ε_{20}, respectively, extrapolate into -2.90 and -2.76 K, quite compatible with the solvation energy of -2.79 K for ^{3}He impurities into liquid ^{4}He.[24]

The effects of curvature can be visualized in Fig. 6, where we plot the chemical potential μ_4 and the ε_{10} energy for the above Au tube in Fig. 5 (thin lines) together with the corresponding energies computed for helium on planar semi-infinite gold (thick lines). Several features appear. First, the behavior of the chemical potential of the ^{4}He atoms reflects, at low coverages, the weakened binding provided by a convex substrate; in fact, in Ref. 17 it has been shown that the minimum of the adsorbing field of an Au solid tube with 12 Å radius is about 70 K higher than for semi-infinite planar gold. Apart from some crossing and moderate oscillations at the intermediate coverages, both chemical potentials merge slightly above $n_4 = 0.4\,\text{Å}^{-2}$ and approach the asymptotic bulk limit. The trend for the smallest coverages is, however, reversed for the binding of the impurity, which shows a substantial gain in the presence of curvature. This is consistent with the drop in the DF results for small N in Fig. 4 and reflects

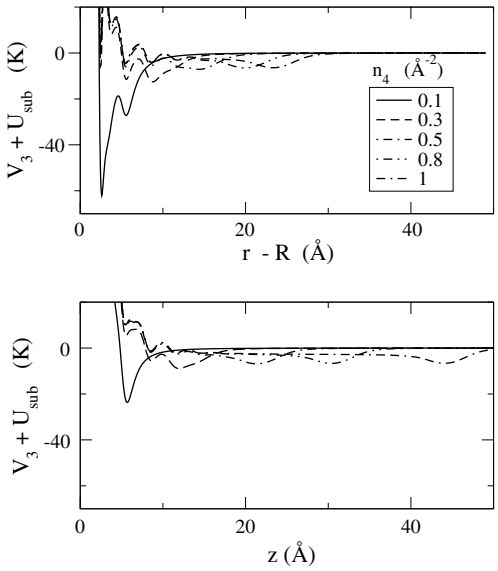

Fig. 7. Total mean field $V_3 + U_{\text{sub}}$ experienced by the single ^{3}He atom in ^{4}He films on Au. Lower panel: planar solid. Upper panel: cylinder.

the influence of the mean field created by the ^{4}He density; to illustrate this point, in Fig. 7 we plot the total mean field plus substrate potential $V_3 + U_{\text{sub}}$ for a gold planar (lower panel) and cylindrical (upper panel) substrate, for various coverages. We observe a pronounced enhancement of the first well minimum for the smallest coverage, $n_4 = 0.1\,\text{Å}^{-2}$, that justifies the high energy gain in the curved substrate field. We also appreciate that if the curvature is nonvanishing, the attractive mean field becomes concentrated in a narrower region, a feature that that is in correspondence with the thinning experienced by the ρ_4 density profiles. To illustrate this point further, in Fig. 8 we plot ^{4}He densities for several cylinder radii and for the planar limit, corresponding to a coverage $n_4 = 0.3\,\text{Å}^{-2}$, as functions of the distance to the curved wall. It is visible in this figure that as the curvature increases, the free surface of the film moves closer to the substrate and some of the outer layers disappear. Corresponding to this situation, all energies of interest, i.e., μ_4, E_{gs}/N and ε_{10} approach smoothly their respectively planar limit as the curvature decreases. The latter results are in agreement with the findings of Ref. 27, where it has been reported that for spherical and cylindrical ^{4}He systems, the surface thickness and tension tend towards their asymptotic planar values when the curvature decreases.

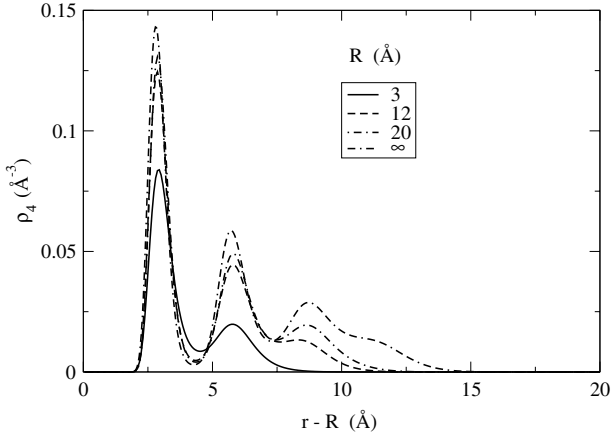

Fig. 8. Density profiles of cylindrical ^{4}He shells on Au cylinders of different radii together with the planar case for a coverage $n_4 = 0.3\,\text{Å}^{-2}$, as functions of the distance to the curved wall.

4. SUMMARY AND CONCLUSIONS

In this work, we take one step forward in our current investigations of adsorption of helium isotopes on curved substrates within FRDF theory, and present the first results concerning structure and energetics of a single ^{3}He atom in ^{4}He shells. We start with spherical films surrounding a C_{60} fullerene, previously described in Refs. 15 and 16, and find that the same overall picture and analysis hold for cylindrical shells in the field of metallic nano-wires, like those recently discussed in Ref. 17. From the qualitative viewpoint, the energetics of ^{3}He binding to the adsorbed ^{4}He film looks identical to that previously encountered for ^{3}He–^{4}He$_N$ systems.[14] In particular, in all cases, we find bulk limits for the gs and first excited sp energies $\varepsilon_{n0}, n = 1$ and 2, respectively, consistent with the energy of the Andreev state, around -5 K, and with the solvation energy -2.79 K of a single ^{3}He atom into liquid ^{4}He. Whichever the substrate, its presence and the characteristics of the confining field, including the geometry, are irrelevant for sufficiently large amounts of ^{4}He, as one could expect. The main effect of very large radii is to weaken the binding of the ^{3}He atom, with a correction linear in the small curvature.

By contrast, the details of the adsorbing potential and type of curvature are significant for the smallest spherical helium systems and for the lowest coverages in the case of cylindrical shells. This has been verified for gold nano-wires, where we have compared the structure and energetics with those predicted for the semi-infinite solid. For cylindrical ^{4}He

shells on Au tubes, we observe a strong compression of the density profiles which, in turn, give rise to compression and deepening of the mean potential experienced by the impurity. This justifies the large binding of the single ^{3}He atom in small clusters and thin shells.

To our belief, the present work contributes to the understanding of various features of helium adsorption on curved surfaces. It should be kept in mind that calculation based on DF for ^{3}He and mixed helium systems should be regarded as indicative, rather than conclusive; in fact, these DF's are parametrized so as to reproduce thermodynamic properties of pure liquid ^{3}He and of the homogeneous solutions, so that the simple parabolic form of the effective mass of the ^{3}He atoms does not take into account several dynamical effects which may become manifest in finite systems. However, the FRDF theory and machinery permits a systematic, semiquantitative investigation of the effects here discussed, with emphasis in the competition between curvature and substrate strength. In particular, concave geometries enhance the depth of the adsorption potential, permitting a decrease of the wetting temperature that may even give rise to zero-temperature wetting. Research along this line and on adsorption of ^{3}He-^{4}He mixtures is in progress and will be reported somewhere.

ACKNOWLEDGMENTS

This work was supported in part by the Ministry of Culture and Education of Argentina through Grants PICT-2000-03-08450 from Agencia Nacional para la Promoción de la Ciencia y la Tecnología, X298 from University of Buenos Aires and PIP's 2391/00 and 2618/00 from Consejo National de Investigaciones Científicas y Técnicas.

REFERENCES

1. *Microscopic Approaches to Quantum Liquids in Confined Geometries*, E. Krotscheck and J. Navarro, eds., World Scientific, Singapore (2002).
2. D. O. Edwards and W. F. Saam, *Progress in Low Temperature Physics*, D. F. Brewer, ed., North Holland, Amsterdam, Vol. VII A, p. 283, (1978).
3. M. Hartmann, R. B. Miller, J. P. Toennies, and A. Vilesov, *Phys. Rev. Lett.* **75**, 1566 (1995).
4. M. A. McMahon, R. N. Barnett, and K. B. Whaley, *J. Chem. Phys.* **104**, 5080 (1996).
5. S. M. Gatica, E. S. Hernández, and M. Barranco, *J. Chem. Phys.* **107**, 927 (1997).
6. A. F. Andreev, *Zh. Eksp. Teor. Fiz.* **50**, 1415 (1966); *Sov. Phys. JETP* **23**, 939 (1966).
7. E. Krotscheck, *Phys. Rev. B* **32**, 5713 (1985).
8. E. Krotscheck, M. Saarela, and J. L. Epstein, *Phys. Rev. B* **38**, 111 (1988).
9. B. E. Clements, E. Krotscheck, and M. Saarela, *Phys. Rev. B* **55**, 5959 (1997).
10. N. Pavloff and J. Treiner, *J. Low. Temp. Phys.* **83**, 331 (1991).
11. F. Dalfovo, *Z. Phys. D* **14**, 263 (1989).
12. E. S. Hernández and J. Navarro, in Ref. 1, pp. 261.
13. A. Belić, F. Dalfovo, S. Fantoni, and S. Stringari, *Phys. Rev. B* **49**, 15253 (1994).

14. M. Barranco, M. Pi, S. M. Gatica, E. S. Hernández, and J. Navarro, *Phys. Rev. B* **56**, 8997 (1997).
15. E. S. Hernández, M. W. Cole, and M. Boninsegni, *Phys. Rev. B* **68**, 125418 (2003).
16. L. Szybisz and I. Urrutia, *J. Low. Temp. Phys.* **134**, 1079 (2004).
17. E. S. Hernández, *J. Low Temp. Phys.* (2004) in press.
18. F. Dalfovo, A. Lastri, L. Pricaupenko, S. Stringari, and J. Treiner, *Phys. Rev. B* **52**, 1193 (1995).
19. M. Pi, R. Mayol, and M. Barranco, *Phys. Rev. Lett.* **82**, 3093 (1999).
20. R. Mayol, M. Pi, M. Barranco, and F. Dalfovo, *Phys. Rev. Lett.* **87**, 145301 (2001).
21. M. Barranco, M. Guilleumas, E. S. Hernández, R. Mayol, M. Pi, and L. Szybisz, *J. Low Temp. Phys.* **136**, 139 (2004).
22. R. Mayol, M. Barranco, E. S. Hernández, M. Pi and M. Guilleumas, *Phys. Rev. Lett.* **90**, 185301 (2003).
23. S. M. Gatica, E. S. Hernández and L. Szybisz, *Phys. Rev. B* **68**, 144501 (2003)
24. C. Ebner and D. O. Edwards, *Phys. Rep.* **2**, 77 (1970).
25. M. Barranco, E. S. Hernández, R. Mayol, and M. Pi, *Phys. Rev. B* **69**, 134502 (2004).
26. M. Boninsegni and L. Szybisz, *Phys. Rev. B* **70**, 024512 (2004).
27. L. Szybisz and I. Urrutia, *Phys. Rev. B* **68**, 054518 (2003).